Supplementary Information

Wrong Expectation of Superinsulation Behavior from Largely-Expanded Nanocellular Foams

Piyapong Buahom,[1] Chongda Wang,[1] Mohammed Alshrah,[1] Guilong Wang[1,2], Pengjian Gong,[1,3] Minh-Phuong Tran,[1,4] Chul B. Park[1,*]

[1]*Microcellular Plastics Manufacturing Laboratory (MPML), Department of Mechanical & Industrial Engineering, University of Toronto, 5 King's College Road, Toronto, M5S 3G8, Ontario, Canada*

[2]*Cellular Polymer Science & Technology Laboratory, School of Materials Science & Engineering, Shandong University, 250061, Shandong, China*

[3]*College of Polymer Science and Engineering, Sichuan University, 610065, Chengdu, China*

[4]*University Grenoble Alpes, CEA, LETI, 17 Avenue des Martyrs, 38000, Grenoble, France*

**Corresponding Author: park@mie.utoronto.ca*

S1 The Conductive Thermal Conductivity

S1.1 Conductive Thermal Conductivity of Cell Walls and Struts

The conductive thermal conductivities of cell walls $k_{\mathrm{c,wall}}$ and struts $k_{\mathrm{c,strut}}$ were determined by analyzing the thermal resistance circuit of heat conduction based on the parallel-series and series-parallel methods for cubic foams.[S1] The parallel-series model regards the material as being made up of parallel columns or sheets of the different phases equivalent to parallel thermal resistance circuit whereas the series-parallel model consists of layers in series equivalent to series thermal resistance circuit. Existing mathematical expressions for these conductive thermal conductivities were presented in several conventions, including: (i) expressions in terms of the void fraction, the material's intrinsic solid-to-gas thermal conductivity ratio;[S2] (ii) expressions in terms of the void fraction, the thermal conductivity of gas, and the thermal conductivity of solid;[S1] (iii) expressions in terms of the foam's geometrical configuration (the cell size and cell wall thickness for closed-cell foams, and the cell size and strut thickness for open-cell foams), the thermal conductivity of gas, and the thermal conductivity of solid;[S3,S4] (iv) expressions in terms of the foam's geometrical configuration and the gas-to-solid thermal conductivity ratio.[S3] Amongst the material's intrinsic parameters, the gas-to-solid thermal conductivity ratio is suitable for the calculation of heat conduction solely through the solid phase, i.e., taking the ratio to 0 to represent the foam under the vacuum condition at a given void fraction. A new set of expressions for the conductive thermal conductivity in terms of the void fraction and the gas-to-solid thermal conductivity ratio are introduced in **Table 1**.

S1.2 Thermal Conductivity of Gas: The Knudsen Effect

The thermal conductivity of gas inside a cell was determined by taking the Knudsen effect[S5] into account, which causes the thermal conductivity of the gas to significantly decrease. In a confined space,

translation of gas molecules is governed by the Knudsen regime, in which the influence of cell size and mean free path on the efficiency of energy transfer is considered.[S3,S6–S8]

$$k_{\mathrm{g}} = \frac{k_{\mathrm{g,bulk}}}{1+2\beta Kn} \tag{S1}$$

where $Kn = \ell_{\mathrm{mean}}/d$ is the Knudsen number, which refers to the ratio of the mean free path ℓ_{mean} of the gas (68 nm for air at 300 K and 1 bar)[S7] to the cell size d. β indicates the energy interaction between gaseous molecules and the solid surface (1.94 for air at 300 K and 1 bar).[S6,S7]

S2. Fundamentals of Mie Theory and Radiative Energy Attenuation

S2.1 Lorenz-Mie-Debye Theory

In thermal insulation foam, radiation in the form of electromagnetic waves propagates through space and interacts with molecules of gas and polymer. Each photon carries a single discrete quantum of thermal radiation and influences electrons in the matter's molecules to increase their energy levels, before some of those exciting electrons release their excess energy and emit photons in a spectrum of wavelengths based on Planck's law of blackbody emission.[S9–S11] Electromagnetic wave phenomena occur when the ray of photons interact with the matter. Some of the radiative energy may be reflected by the surface while the remainder penetrates the medium, where the radiative energy can be partially or completely absorbed. Multiple internal reflection, diffraction, scattering, absorption and re-emission occur in the foam structure of thermal insulation, leading to a tortious transport path of radiative energy transfer.[S11,S12] In such complicated energy-matter interaction in foam, scattering and absorption makes a substantial contribution to attenuation of the radiative energy.

Scattering can be explained by the well-established Lorenz-Mie-Debye theory, also called Mie theory or Lorenz-Mie theory.[S11,S13–S16] It is an analysical solution of Maxwell's electromagnetic equations, which encompass the major laws of electricity and magnetism, for the scattering of a plane wave of electromagnetic radiation by a homogeneous dielectric spherical particle. It is worth noting that

Mie scattering is theoretical rather than a physical phenomenon. Mie scattering theory assumes that the oscillating electric field of the incident photon acts on the charges (i.e., electrons) within the particles, causing the charges to move at the same frequency and, therefore, to become small radiating dipoles, which radiate in various directions as scattered waves. This radiation is an integral part of the incident energy, and no frequency change occurs due to excitation or deexcitation. It is considered an elastic scattering process, in which the frequency (and thereby the wavelength) of the electromagnetic waves is not substantially changed. As **Figure S1a** shows, the plot between the extinction efficiency, i.e., the ratio of the extinction cross-section to the geometric-cross-section, and the size parameter $x = 2\pi r_{\mathrm{scatter}}/\lambda$, which depends on the scatterer's radius r_{scatter} and the wavelength λ, can be considered in three regimes: (i) When the scatterer's size is relatively small compared to a wavelength, i.e., $x < 0.1$, (ii) relatively moderate, i.e., $0.1 < x < 50$, and (iii) relatively large, i.e., $x > 50$.[S17,S18] When the scatterer's radius is relatively small compared to the wavelength (① in **Figure S1a**), the Mie scattering gives similar results to Rayleigh scattering theory[S19] (the dashed line in **Figure S1a**), which shows a symmetric scattering envelope in the forward and backward directions, as shown in **Figure S1b**. As one of the limiting cases of Mie scattering, Rayleigh scattering, sometimes referred to as a molecular or particle scattering, does not involve internal interference. When the scatterer's radius is increased (② in **Figure S1a**), the combined interference effects from each scattering point inside the scatterer produces the Mie solution, which varies sinusoidally. There is a departure from symmetry, more scattered energy in the forward direction than in the opposite direction. When the scatterer's radius is relatively large compared to the wavelength (③ in **Figure S1a**), the Mie scattering is similar to geometric optics,[S20,S21] also known as ray optics,[S22–S24] in which reflection and refraction can be analyzed by simple geometry, assuming that the incident beam propagates in straight-line paths without considering electromagnetic wave effects such as diffraction and interference, as shown in **Figure S1c**. Scattering by a cylinder,[S19,S25–S28]

spheroid,[S28–S31] prismatic column,[S32–S34] and platelet[S35,S36] can be determined by an equivalent solution to the Mie scattering by a sphere.

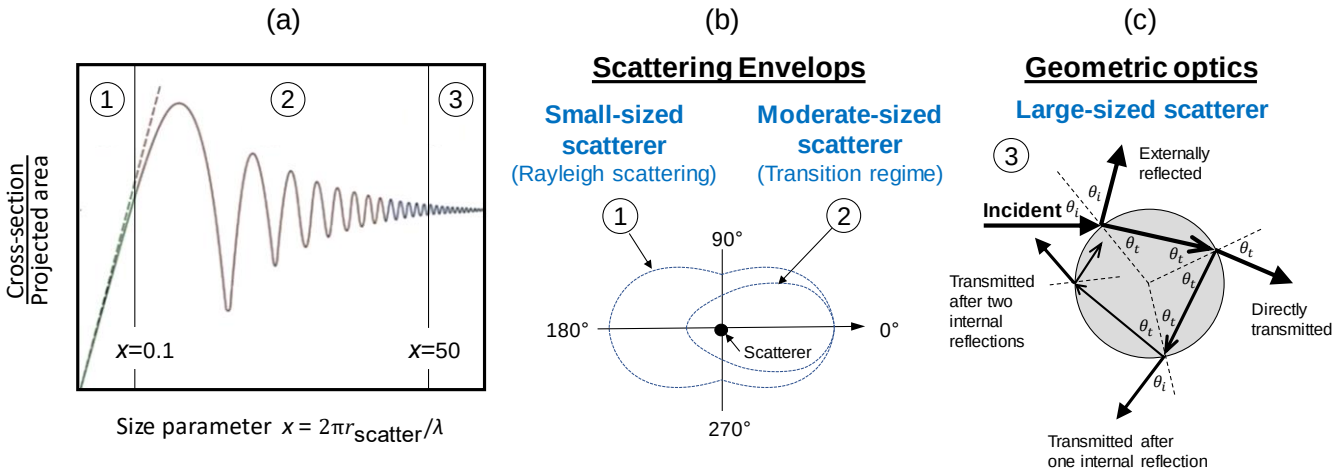

Figure S1. (a) The extinction efficiency for scattering of a plane wave of electromagnetic radiation through a homogeneous sphere in ① Raleigh scattering, ② transition and ③ geometric optics regimes; (b) Symmetric scattering envelope in Rayleigh scattering for relatively large wavelengths and asymmetric scattering envelope for relatively moderate wavelengths; and (c) Geometric optics for relatively small wavelengths.

S2.2 Cross-sections

Attenuation of the radiative energy due to scattering can be quantified by scattering cross-section. Considering a parallel beam of electromagnetic waves with a flux density F_{in} along the incident direction shining on a particle, as shown in **Figure S2a**, the scattered beam of waves is measured within a small cone of solid angle dΩ, along a direction which makes an angle θ with the incident beam. The angle θ is known as the "scattering angle".[S11,S15] The intensity of the scattered beam, which is the scattered energy flux per solid angle, along the direction (θ, φ) is: $I_\lambda^{(\text{sca})} = d\Phi_\lambda^{(\text{sca})}/d\Omega$. Assume that the particle is a homogeneous sphere, to comform to Mie theory. To simplify the scattering geometry, the z-axis is

directed along the direction of the incident flux with the origin at the center of the particle. By azimuthal symmetry, the scattered intensity depends only on the scattering angle θ of the spherical coordinate system,[S11] meaning that $I_{\lambda}^{(\mathrm{sca})}(\theta,\varphi) = I_{\lambda,\theta}^{(\mathrm{sca})}(\theta)$.

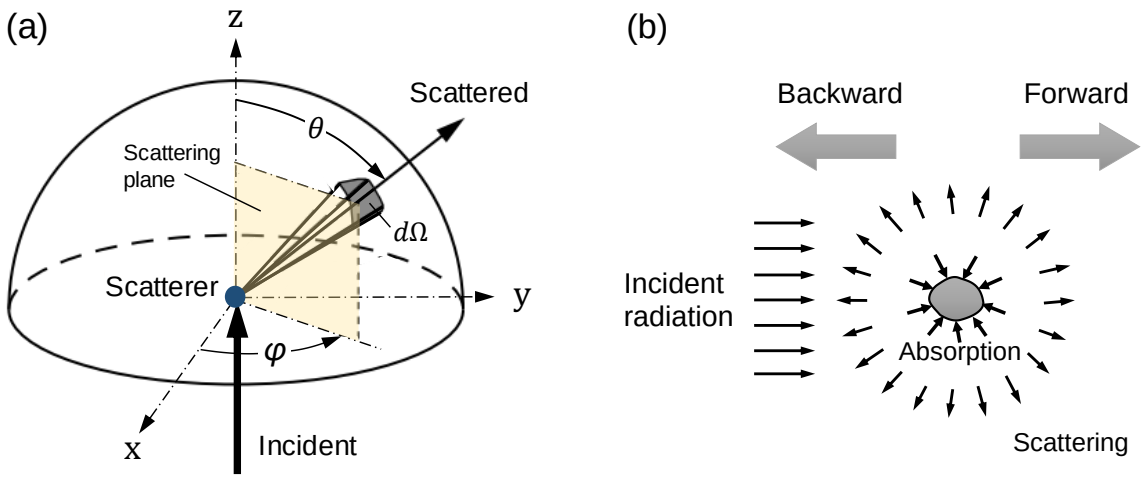

Figure S2. (a) Incident and scattered beams of radiation, (b) Geometrical and effective extinction cross-sections, (c) Radiative energy attenuation due to absorption and scattering.

The ratio of the scattered flux intensity $I_{\lambda,\theta}^{(\mathrm{sca})}$ to the incident energy flux F_{in} is the angular scattering cross-section:

$$C_{\lambda,\theta}^{(\mathrm{sca})}(\theta) = \frac{I_{\lambda,\theta}^{(\mathrm{sca})}(\theta)}{F_{\mathrm{in}}} = \frac{d\Phi_{\lambda}/d\Omega}{F_{\mathrm{in}}} \tag{S2}$$

By integrating over all solid angles, the spectral scattering cross-section is obtained.

$$C_{\lambda}^{(\mathrm{sca})} = \int C_{\lambda,\theta}^{(\mathrm{sca})}\, d\Omega = \int_0^{2\pi}\int_0^{\pi} C_{\lambda,\theta}^{(\mathrm{sca})} \sin\theta\, d\theta\, d\varphi = 2\pi \int_0^{\pi} C_{\lambda,\theta}^{(\mathrm{sca})} \sin\theta\, d\theta \tag{S3}$$

It is worth noting that the total power removed from the monochromatic incident radiation due exclusively to scattering can be obtained by the product of the scattering cross-section $C_{\lambda}^{(\mathrm{sca})}$ and the incident energy flux F_{in}.[S37]

For an absorbing material, which has a non-zero imaginary part of the spectral refractive index κ_λ, the total power absorbed per unit incident energy flux is defined as the spectral absorption cross-section $C_\lambda^{(\mathrm{abs})}$.

Because attenuation of the incident beam of electromagnetic waves is due to scattering and absorption, as shown in **Figure S2b**, the first law of thermodynamics gives the total flux of energy attenuated.[S11]

$$q_\lambda^{(\mathrm{ext})} = q_\lambda^{(\mathrm{sca})} + q_\lambda^{(\mathrm{abs})} \tag{S4}$$

Because the geometric cross-section is constant, the spectral extinction cross-section is the sum of the scattering and absorption cross-sections.[S11]

$$C_\lambda^{(\mathrm{ext})} = C_\lambda^{(\mathrm{abs})} + C_\lambda^{(\mathrm{sca})} \tag{S5}$$

When multiplied by the energy flux of incident monochromatic, the spectral extinction cross-section $C_\lambda^{(\mathrm{ext})}$ gives the total power removed from the incident radiation due to both scattering and absorption.[S37]

S2.3 Efficiency Factors

The ratio of the spectral scattering cross-section $C_\lambda^{(\mathrm{sca})}$ to the geometric cross-section $C^{(\mathrm{geo})}$ of the particle defines the spectral scattering efficiency factor $Q_\lambda^{(\mathrm{sca})}$.[S38,S39]

$$Q_\lambda^{(\mathrm{sca})} = \frac{C_\lambda^{(\mathrm{sca})}}{C^{(\mathrm{geo})}} = \frac{P_\lambda^{(\mathrm{sca})}}{P_{\mathrm{in}}^{(\mathrm{geo})}} \tag{S6}$$

This quantity indicates the energy power $P_\lambda^{(\mathrm{sca})} = C_\lambda^{(\mathrm{sca})} F_{\mathrm{in}}$ removed due to scattering from the power of the incident ray that projects onto the geometrical cross-section $P_{\mathrm{in}}^{(\mathrm{geo})} = C^{(\mathrm{geo})} F_{\mathrm{in}}$.

Similarly, the spectral absorption efficiency coefficient for an absorbing material is:

$$Q_\lambda^{(\mathrm{abs})} = \frac{C_\lambda^{(\mathrm{abs})}}{C_{\mathrm{scatter}}^{(\mathrm{geo})}} = \frac{P_\lambda^{(\mathrm{abs})}}{P_{\mathrm{in}}^{(\mathrm{geo})}} \tag{S7}$$

This quantity indicates the energy power $P_\lambda^{(\mathrm{sca})} = C_\lambda^{(\mathrm{abs})} F_{\mathrm{in}}$ absorbed from the power of the incident ray that projects onto the geometrical cross-section.

Because the same A_{scatter} is considered, the spectral extinction efficiency factor becomes:

$$Q_\lambda^{(\mathrm{ext})} = Q_\lambda^{(\mathrm{abs})} + Q_\lambda^{(\mathrm{sca})} \tag{S8}$$

Thus, the spectral extinction efficiency factor becomes:

$$Q_\lambda^{(\mathrm{ext})} = \frac{C_\lambda^{(\mathrm{ext})}}{C_{\mathrm{scatter}}^{(\mathrm{geo})}} = \frac{P_\lambda^{(\mathrm{ext})}}{P_{\mathrm{in}}^{(\mathrm{geo})}} \tag{S9}$$

The extinction efficiency factor indicates the extincted power $P_\lambda^{(\mathrm{ext})}$ removed, due to both scattering and absorption, from the power of the incident beam $P_{\mathrm{in}}^{(\mathrm{geo})}$. It is worth noting that the scattering, absorption and extinction cross-sections are dependent on the particle size.

S2.4 Spectral Extinction Coefficient

Considering that an incident beam encounters randomly oriented scatterers at various oblique incident angles ϕ, which is the angle between the incoming incident ray and the scatterer's normal direction, the spectral extinction cross-section represents attenuation of the incident beam due to both absorption and scattering. The mathematical description of the apparent spectral scattering cross-section $\langle C_\lambda^{(\mathrm{sca})} \rangle$ and the apparent spectral extinction cross-section $\langle C_\lambda^{(\mathrm{ext})} \rangle$ is applied, respectively, for the apparent scattered energy and total attenuated energy with respect to the incident direction:[S40]

$$\langle C_\lambda^{(\mathrm{sca})} \rangle = \int_0^{\pi/2} C_\lambda^{(\mathrm{sca})} \cos\phi \sin\phi \, d\phi \tag{S10}$$

$$\langle C_\lambda^{(\mathrm{ext})} \rangle = \int_0^{\pi/2} C_\lambda^{(\mathrm{ext})} \cos\phi \sin\phi \, d\phi \tag{S11}$$

The spectral extinction and scattering coefficients of the scatterer are thus defined by:

$$\beta_\lambda = N_{\mathrm{v,scatter}} \langle C_\lambda^{(\mathrm{ext})} \rangle \tag{S12}$$

$$\sigma_\lambda = N_{\mathrm{v,scatter}} \langle C_\lambda^{(\mathrm{sca})} \rangle \tag{S13}$$

where $N_{\mathrm{v,scatter}}$ is the number density of scatterers. For normal incidence, $\phi = 0$, the incoming incident beam is perpendicular to the surface of the scatterer, meaning that $\langle C_\lambda^{(\mathrm{sca})} \rangle = C_\lambda^{(\mathrm{sca})}$ and $\langle C_\lambda^{(\mathrm{ext})} \rangle = C_\lambda^{(\mathrm{ext})}$.

Attenuation or extinction is the gradual loss of the radiative energy through a medium due to interaction between the incident electromagnetic waves and the matter. Defined as attenuation of the incident energy due to absorption and scattering at a specific wavelength λ, the spectral extinction coefficient β_λ can be considered as the sum of the absorption coefficient κ_λ and the scattering coefficient σ_λ.

$$\beta_\lambda = \kappa_\lambda + \sigma_\lambda \tag{S14}$$

S2.5 Asymmetry Factor and Effective Spectral Extinction Coefficient

Due to the non-isotropic nature of scattering in foams, unlike absorption, scattering can be apportioned into directions. The fraction of the energy transmitted in the forward direction can be described by the asymmetry factor g_λ. The effective spectral extinction coefficient $\beta_\lambda^{(\mathrm{eff})}$, including absorption and scattering in the backward direction (**Figure S2b**), can be determined:

$$\beta_\lambda^{(\mathrm{eff})} = \kappa_\lambda + \sigma_\lambda(1 - g_\lambda) \tag{S15}$$

Inserting Equation (S14), this becomes:[S41,S42]

$$\beta_\lambda^{(\mathrm{eff})} = \beta_\lambda - g_\lambda \sigma_\lambda \tag{S16}$$

where the term $g_\lambda \sigma_\lambda$ represents the scattered energy in the forward direction. Equation (S16) will be applied for the effective spectral extinction coefficients of struts and cell walls.

The asymmetry factor g_λ of the scatterer is can be obtained from:[S43]

$$g_\lambda = \frac{\int_0^\pi P_\lambda^{(\mathrm{sca})} \cos\theta \, d\theta}{\int_0^\pi P_\lambda^{(\mathrm{sca})} d\theta} \tag{S17}$$

where the scattering phase function $P_\lambda^{(\mathrm{sca})}$ for mono-dispersion particles, which describes the angle-dependent scattering of the incident beam, is defined by:

$$P_\lambda^{(\mathrm{sca})} = 4\pi \frac{\sigma_{\lambda,\theta}}{\sigma_\lambda} \tag{S18}$$

and the angular scattering coefficient of the scatterer $\sigma_{\lambda,\phi}$ is the product of the number density N_{scatter} and the angular scattering cross-section $C_{\lambda,\theta}^{(\mathrm{sca})}$:

$$\sigma_{\lambda,\theta} = N_{\mathrm{scatter}} C_{\lambda,\theta}^{(\mathrm{sca})} \tag{S19}$$

Thus, the asymmetry factor becomes:[S40,S43]

$$g_\lambda = \frac{\int_0^\pi C_{\lambda,\theta}^{(\mathrm{sca})} \cos\theta d\theta}{\int_0^\pi C_{\lambda,\theta}^{(\mathrm{sca})} d\theta} = \frac{\int_0^\pi I_\lambda^{(\mathrm{sca})} \cos\theta d\theta}{\int_0^\pi I_\lambda^{(\mathrm{sca})} d\theta} \tag{S20}$$

It is worth to not that and $g_\lambda = 0$ for symmetric scattering, and the asymmetry factor of a cylinder can reach negative values when it is predominant back scattering.

The asymmetry factor of struts was calculated by using Equation (S20) and the intensity of the scattered wave includes the incident in TM and TE cases:[S38,S44,S45]

$$I_\lambda^{(\mathrm{sca})}(\theta) = \frac{I_\lambda^{(\mathrm{TM})} + I_\lambda^{(\mathrm{TE})}}{2} \tag{S21}$$

and each case includes the scattered energy in both cases I and II. These quantities can be obtained using the optical theorem:

$$I_\lambda^{(\mathrm{TM})} = \frac{2}{\pi x}\left(\left|b_0^I + 2\sum_{n=1}^{\infty} b_n^I \cos(n\theta)\right|^2 + \left|2\sum_{n=1}^{\infty} a_n^I \sin(n\theta)\right|^2\right) \tag{S22}$$

$$I_\lambda^{(\mathrm{TE})} = \frac{2}{\pi x}\left(\left|a_0^{II} + 2\sum_{n=1}^{\infty} a_n^{II} \cos(n\theta)\right|^2 + \left|2\sum_{n=1}^{\infty} b_n^{II} \sin(n\theta)\right|^2\right) \tag{S23}$$

where the coefficients $a_{\mathrm{n}}^{\mathrm{H}}$, $a_{\mathrm{n}}^{\mathrm{E}}$, $b_{\mathrm{n}}^{\mathrm{H}}$ and $b_{\mathrm{n}}^{\mathrm{E}}$ depend on (i) the complex refractive index $m=n+ik$, (ii) size parameter $x = \pi d_{\mathrm{s}}/\lambda$, which is dependent on the strut diameter d_{s} and wavelength λ, and (iii) the incident angle. The expressions for these coefficiencs can be found in Ref. [S27], which implements the ratio algorithm for the computation of cylindrical functions in Ref. [S46].

S3 Calculation of the Effective Spectral Extinction Coefifcient of Cell Walls

S3.1 Derivation of the newly developed model for $\beta_{\lambda,\mathrm{wall}}^{(\mathrm{eff})}$

Considering attenuation of thermal radiation by randomly oriented cell walls in the foam, each cell wall is assumed as an isolated platelet that attenuates the incident beam independently from each other. From Equation (S12), the spectral extinction coefficient of cell wall can be determined in terms of the number density of cell walls and the extinction capability of each cell wall, as follows:

$$\beta_{\lambda,\mathrm{wall}} = N_{\mathrm{v,wall}}\langle C_{\lambda,\mathrm{wall}}^{(\mathrm{ext})}\rangle \tag{S24}$$

where $N_{\mathrm{v,wall}}$ is the number of cell walls per unit volume of foam, and $\langle C_{\lambda,\mathrm{wall}}^{(\mathrm{ext})}\rangle$ is the apparent spectral extinction cross-section of cell wall obtained by averaging the spectral extinction cross-section of cell wall over incidence angles from 0 to π/2:

$$\langle C_{\lambda,\mathrm{wall}}^{(\mathrm{ext})}\rangle = \int_0^{\pi/2} C_{\lambda,\mathrm{wall}}^{(\mathrm{ext})}\cos\phi_1\sin\phi_1 d\phi_1 \tag{S25}$$

where $C_{\lambda,\mathrm{wall}}^{(\mathrm{ext})}$ is the spectral extinction cross-section of cell wall for the incident beam interacts with a wall tilted by the incidence angle ϕ_1 measured away from the surface's normal (**Figure 1b**). Because the spectral extinction efficiency factor is defined as the ratio of the spectral extinction cross-section to the geometric cross-section of cell wall at normal incident, $Q_\lambda^{(\mathrm{ext})} = C_{\lambda,\mathrm{wall}}^{(\mathrm{ext})}/C_{\mathrm{wall}}^{(\mathrm{geo})}$, the spectral extinction coefficient of cell wall becomes:

$$\beta_{\lambda,\mathrm{wall}} = N_{\mathrm{v,wall}}C_{\mathrm{wall}}^{(\mathrm{geo})}\int_0^{\pi/2} Q_{\lambda,\mathrm{wall}}^{(\mathrm{ext})}\cos\phi_1\sin\phi_1 d\phi_1 \tag{S26}$$

where the geometric cross-section of cell wall is equal to the average surface area of cell wall.

When the incident beam projects on the surface of a cell wall, part of the incident energy may be reflected from the surface, absorbed by the polymer molecules and transmitted through the cell wall. Accordingly, the fraction of the radiative energy reflected, absorbed and transmitted at a wavelength λ in the radiation spectrum can be defined as the spectral reflectivity (A_λ), spectral absorptivity (R_λ) and

spectral transmissivity (T_λ) of cell wall, respectively. For monochromic radiation, the sum of these fractions must equal to unity.[S6,S15]

$$A_{\lambda,\mathrm{wall}} + R_{\lambda,\mathrm{wall}} + T_{\lambda,\mathrm{wall}} = 1 \tag{S27}$$

Assuming the energy absorbed by each cell wall is emitted in thermodynamic equilibrium, based on Kirchhoff's law of thermal radiation,[S47–S49] the fraction of energy emitted from a cell wall is equal to the fraction of energy absorbed by the cell wall, i.e., the spectral emissivity of cell wall equals the spectral absorptivity of cell wall. Because of thin cell walls in microcellular and nanocellular foams, the temperature profile across the thickness of a cell wall can be assumed as uniform. At the same surface temperature, the absorbed energy is emitted equally from both sides of the cell wall.

The net fraction of energy sent backward, including the reflected energy and half of the absorbed energy emitted in the backward direction can be considered as attenuation of the incident beam. Correspondingly, the spectral extinction efficiency factor of cell wall ($Q_{\lambda,\mathrm{wall}}^{(\mathrm{ext})}$), which indicates the fraction of energy attenuated, can be obtained by the sum of the spectral reflectivity and half of the spectral absorptivity of cell wall.

$$Q_{\lambda,\mathrm{wall}}^{(\mathrm{ext})} = R_{\lambda,\mathrm{wall}} + \frac{1}{2} A_{\lambda,\mathrm{wall}} \tag{S28}$$

Because $A_{\lambda,\mathrm{wall}} = 1 - R_{\lambda,\mathrm{wall}} - T_{\lambda,\mathrm{wall}}$, the effective spectral extinction coefficient of cell wall becomes:

$$\beta_{\lambda,\mathrm{wall}}^{(\mathrm{eff})} = N_{\mathrm{v,wall}} C_{\mathrm{wall}}^{(\mathrm{geo})} \int_0^{\pi/2} \left(1 + R_{\lambda,\mathrm{wall}} - T_{\lambda,\mathrm{wall}}\right) \frac{\sin(2\phi_1)}{4} d\phi_1 \tag{S29}$$

S3.2 Calculation of the Spectral Reflectivity and Spectral Transmittivity of Cell Wall

For each mode of the incident wave in the transverse magnetic (TM) and transverse electric (TE) modes, the spectral reflectivity $R_{\lambda,\mathrm{wall}}$ and spectral transmissivity $T_{\lambda,\mathrm{wall}}$ of a polymer film were calculated based on Fresnel formulae for an absorbing film considering the interference effects.[S3,S15]

$$R_{\lambda,\mathrm{wall}} = \frac{\rho_{\lambda,\mathrm{gs}}^2 + \rho_{\lambda,\mathrm{sg}}^2 + 2\rho_{\lambda,\mathrm{gs}}\rho_{\lambda,\mathrm{sg}} \cos 2\widetilde{\beta}_\lambda}{1 + \rho_{\lambda,\mathrm{gs}}^2 \rho_{\lambda,\mathrm{sg}}^2 + 2\rho_{\lambda,\mathrm{gs}}\rho_{\lambda,\mathrm{sg}} \cos 2\widetilde{\beta}_\lambda} \tag{S30}$$

$$T_{\lambda,\mathrm{wall}} = \frac{\tau_{\lambda,\mathrm{gs}}^2 \tau_{\lambda,\mathrm{sg}}^2}{1+\rho_{\lambda,\mathrm{gs}}^2 \rho_{\lambda,\mathrm{sg}}^2 + 2\rho_{\lambda,\mathrm{gs}}\rho_{\lambda,\mathrm{sg}} \cos 2\tilde{\beta}_\lambda} \quad \text{(S31)}$$

The spectral reflection and transmission coefficients at the gas-solid ($\rho_{\lambda,\mathrm{gs}}$, $\tau_{\lambda,\mathrm{gs}}$) and solid-gas ($\rho_{\lambda,\mathrm{sg}}$, $\tau_{\lambda,\mathrm{sg}}$) interfaces were defined as:[S3,S15]

$$\rho_{\lambda,\mathrm{gs}} = \frac{\hat{n}_{\lambda,\mathrm{g}} \cos\phi_1 - \hat{n}_{\lambda,\mathrm{s}} \cos\phi_2}{\hat{n}_{\lambda,\mathrm{g}} \cos\phi_1 + \hat{n}_{\lambda,\mathrm{s}} \cos\phi_2} \quad \text{(S32)}$$

$$\rho_{\lambda,\mathrm{sg}} = -\rho_{\lambda,\mathrm{gs}} \quad \text{(S33)}$$

$$\tau_{\lambda,\mathrm{gs}} = \frac{2\hat{n}_{\lambda,\mathrm{g}} \cos\phi_1}{\hat{n}_{\lambda,\mathrm{g}} \cos\phi_1 + \hat{n}_{\lambda,\mathrm{s}} \cos\phi_2} \quad \text{(S34)}$$

$$\tau_{\lambda,\mathrm{sg}} = \frac{2\hat{n}_{\lambda,\mathrm{s}} \cos\phi_2}{\hat{n}_{\lambda,\mathrm{g}} \cos\phi_1 + \hat{n}_{\lambda,\mathrm{s}} \cos\phi_2} \quad \text{(S35)}$$

The spectral complex refractive indices of polymer film and non-absorbing gas were defined as $\hat{n}_{\lambda,\mathrm{s}} = n_{\lambda,\mathrm{s}} + i\kappa_{\lambda,\mathrm{s}}$ and $\hat{n}_{\lambda,\mathrm{g}} = n_{\lambda,\mathrm{g}}$. The spectral value of $\tilde{\beta}_\lambda$ and the refractive angle ϕ_2 at the gas-polymer interface were calculated based on Snell's law:[S3,S15]

$$\tilde{\beta}_\lambda = \frac{2\pi d_{\mathrm{wall}}}{\lambda} \hat{n}_{\lambda,s} \cos\phi_2 \quad \text{(S36)}$$

$$\phi_2 = \sin^{-1}\left(\frac{n_{\lambda,g}}{n_{\lambda,s}} \sin\phi_1\right) \quad \text{(S37)}$$

S4 Calculation of the Scattering and Extinction Efficiency Factors of Struts

The extinction efficiency factor $Q_{\lambda,\mathrm{strut,O}}^{(\mathrm{ext})}$ and the scattering efficiency factor $Q_{\lambda,\mathrm{strut,O}}^{(\mathrm{sca})}$ for a cylindrical strut can be split into two incident cases: transverse electric (TE) and transverse magnetic (TM) modes. In the TE mode, the electric field is transverse to the plane of incident, which is the plane that contains the incident ray and the surface's normal vector. In the TM mode, the magnetic field vector is transverse to the plane of incident, i.e. the electric field vector is parallel to the plane of incident. The solutions for the scattered wave are usually further decomposed into two scattered components: the scattered wave in the same mode and in the different mode as the incident wave.

The extinction efficiency factor is obtained by the average of the extinction efficiency factors corresponding to the incident TM and TE modes:

$$Q_{\lambda,\mathrm{strut,O}}^{(\mathrm{ext})} = \frac{Q_{\mathrm{ext}}^{(\mathrm{TM})} + Q_{\mathrm{ext}}^{(\mathrm{TE})}}{2} \tag{S38}$$

where the extinction efficiency factors corresponding to the incident TM and TE modes[S27,S38,S46] are obtained by using the optical theorem:[S27,S38,S46]

$$Q_{\mathrm{ext}}^{(\mathrm{TM})} = \frac{2}{x} Re\{a_0^{\mathrm{H}} + 2\sum_{n=1}^{\infty} a_{\mathrm{n}}^{\mathrm{H}}\} \tag{S39}$$

$$Q_{\mathrm{ext}}^{(\mathrm{TE})} = \frac{2}{x} Re\{b_0^{\mathrm{E}} + 2\sum_{n=1}^{\infty} b_{\mathrm{n}}^{\mathrm{E}}\} \tag{S40}$$

Similarly, the scattering efficiency factor is obtained by the average of the scattering efficiency factors corresponding to the incident TM and TE modes:

$$Q_{\lambda,\mathrm{strut,O}}^{(\mathrm{sca})} = \frac{Q_{\mathrm{sca}}^{(\mathrm{TM})} + Q_{\mathrm{sca}}^{(\mathrm{TE})}}{2} \tag{S41}$$

where

$$Q_{\mathrm{sca}}^{(\mathrm{TM})} = \frac{2}{x}\left(\left|a_0^{\mathrm{H}}\right|^2 + 2\sum_{n=1}^{\infty}(|a_{\mathrm{n}}^{\mathrm{H}}|^2 + |b_{\mathrm{n}}^{\mathrm{H}}|^2)\right) \tag{S42}$$

$$Q_{\mathrm{sca}}^{(\mathrm{TE})} = \frac{2}{x}\left(\left|b_0^{\mathrm{E}}\right|^2 + 2\sum_{n=1}^{\infty}(|a_{\mathrm{n}}^{\mathrm{E}}|^2 + |b_{\mathrm{n}}^{\mathrm{E}}|^2)\right) \tag{S43}$$

S5 Calculation of the Radiative Heat Transfer Coefficient

Based on the fluctuation-dissipation theorem and fluctuational electrodynamics, the radiative heat transfer coefficient at a temperature T was calculated as the contributions of evanescent and propagating modes:[S50–S52]

$$h_{\mathrm{rad}}(T,d) = h_{\mathrm{evan}}(T,d) + h_{\mathrm{prop}}(T,d) \tag{S44}$$

Consider the radiative energy exchange between two polymer layers. Incident photons of various angular frequencies $\omega=2\pi/\lambda$, corresponding to wavelengths in Planck's energy distribution, interact with the surfaces of struts and cell walls at incidence angles varying from 0 to $\pi/2$. To account for the fact that

the foam structure is homogenous, non-magnetic, optically thin and randomly oriented, the contributions from propagating and evanescent modes can be calculated as follows:

$$h_{\mathrm{prop}} = \frac{1}{4\pi^2}\int_0^{\infty}\left(\frac{\partial\Theta(\omega,\mathrm{T})}{\partial T}\int_0^{k_0}\left[S_{\mathrm{prop}}^{\mathrm{TM}}(\omega,k_{\parallel}) + S_{\mathrm{prop}}^{\mathrm{TE}}(\omega,k_{\parallel})\right]dk_{\parallel}\right)d\omega \tag{S45}$$

$$h_{\mathrm{evan}} = \frac{1}{\pi^2}\int_0^{\infty}\left(\frac{\partial\Theta(\omega,\mathrm{T})}{\partial T}\int_{k_0}^{\infty}[S_{\mathrm{evan}}^{\mathrm{TM}}(\omega,k_{\parallel}) + S_{\mathrm{evan}}^{\mathrm{TE}}(\omega,k_{\parallel})]dk_{\parallel}\right)d\omega \tag{S46}$$

where $k_{\parallel} = pk_0$ is the parallel wavevector component along the surface corresponding to various incidence angles, with $k_0 = \omega/\mathrm{c}$ being the magnitude of the wavevector in the separation gap and p being a dimensionless parameter ranged from 0 to infinity. $0 \le p \le 1$ corresponds to propagating waves, whereas $p > 1$ corresponds to evanescent waves. The derivative of the Planck's mean energy of a harmonic oscillator with respect to the temperature is given by:

$$\frac{\partial\Theta(\omega,\mathrm{T})}{\partial T} = \frac{\hbar^2\omega^2 e^{(\hbar\omega/k_BT)}}{k_BT^2\left(e^{(\hbar\omega/k_BT)}-1\right)^2} \tag{S47}$$

where $\hbar = h/2\pi$ is the reduced Planck constant.[S53,S54] For each polarization mode (TM and TE), the exchange functions are used to describe the frequency-dependent correlations of radiative heat transfer for propagating and evanescent waves as follows:

$$S_{\mathrm{prop}}(\omega,k_{\mathrm{p}}) = \left(\frac{1-|R_{\mathrm{m}}|^2-|T_{\mathrm{m}}|^2}{1-|R_{\mathrm{m}}|^2e^{2ik_{\perp,\mathrm{g}}d}}\right)^2 \tag{S48}$$

$$S_{\mathrm{evan}}(\omega,k_{\mathrm{p}}) = k_{\mathrm{p}}\left(\frac{\mathrm{Im}(R_{\mathrm{m}})}{1-|R_{\mathrm{m}}|^2e^{2ik_{\perp,\mathrm{g}}d}}\right)^2 e^{2ik_{\perp,\mathrm{g}}d} \tag{S49}$$

where the reflection coefficient R_{m} and transmission coefficient T_{m} of the material are given as:

$$R_{\mathrm{m}} = \frac{r_{\mathrm{gs}}+r_{\mathrm{sg}}e^{2ik_{\perp,\mathrm{s}}t_s}}{1+r_{\mathrm{gs}}+r_{\mathrm{sg}}e^{2ik_{\perp,\mathrm{s}}t_s}} \tag{S50}$$

$$T_{\mathrm{m}} = \frac{t_{\mathrm{gs}}t_{\mathrm{sg}}e^{ik_{\perp,\mathrm{s}}t_s}}{1+t_{\mathrm{gs}}t_{\mathrm{sg}}e^{2ik_{\perp,\mathrm{s}}t_s}} \tag{S51}$$

where $k_{\perp,\mathrm{g}} = k_0\sqrt{1-p^2}$ and $k_{\perp,\mathrm{s}} = k_0\sqrt{\varepsilon_s - p^2}$ are the component wavevectors perpendicular to the surface in the gap and polymer, respectively, with ε_s being the dielectric constant of the polymer. The

details of the calculation for the Fresnel reflection and transmission coefficients r_{gs}, r_{sg}, t_{gs}, and t_{sg} can be found in Ref. [S52].

S6 Dimension and Number Density of Struts and Cell Walls

S6.1 Cell wall thickness

For a given cell size (d), void fraction (ε) and volume fraction of polymer located in struts (known as strut fraction (F_{strut})), the cell wall thickness (d_w) can be estimated by using the following formula:[S55–S57]

$$d_w = \frac{(1-\varepsilon)(1-F_{\text{strut}})}{c_{12}} d \tag{S52}$$

where $c_{12} = 3.46$ is constant for regular dodecahedral foam.

S6.2 Strut Diameter

The strut diameter (d_s), which is the diameter of volume-equivalent cylindrical strut, can be obtained by solving the following equation:[S42]

$$\frac{(1-VF)0.348-2.8\left(\frac{d_s}{d}\right)^2+3.93\left(\frac{d_s}{d}\right)^3}{1.3143-7.367\left(\frac{d_s}{d}\right)+10.323\left(\frac{d_s}{d}\right)^2} = \frac{(1-\varepsilon)(1-F_{\text{strut}})}{c_{12}} \tag{S53}$$

S6.3 Geometric Cross-section of Cell Walls and Struts

The strut length a_s in the regular dodecahedral cell is calculated by the following correlation:[S58,S59]

$$a_s = 0.4490280d \tag{S54}$$

The geometric cross-section of cell walls is obtained by the average surface area of cell walls, which can be calculated from the surface area of cell walls divided by 12 faces in a regular dodecahedral cell:[S58,S59]

$$C_{wall}^{(geo)} = \frac{3\sqrt{25+10\sqrt{5}}a_s^2}{12} = 0.1156311d^2 \quad \text{(S55)}$$

The geometric cross-section of struts is the area projected normally by incident beam. At the normal incident (ϕ_1=0), the geometric cross-section can be obtained from the diameter (d_s) and the edge length (a_s) of the strut.[S27]

$$C_{\text{strut}}^{(\text{geo})} = d_s a_s \quad \text{(S56)}$$

S6.4 Number Densities of Cell Walls and Struts

The number density of struts and cell walls can be obtained when the cell number density of the foam is determined. The cell number density can be calculated using the correlation of the unit cell's volume corresponding to the critical bubble lattice method:[S60]

$$N_{\text{v,cell}} = \frac{N_{\text{cell}}}{V_{\text{foam}}} = \frac{1}{\bar{V}_{\text{cell}}} = \frac{\chi}{(d+d_w)^3} \quad \text{(S57)}$$

where N_{cell} is the number of cells in the volume of foam V_{foam}, and $\bar{V}_{\text{cell}}$ is the average cell volume of each cell, for which the diameter of the insphere $d_{\text{ins}} = d + d_{\text{w}}$ is dependent on the cell size (d) and cell wall thickness (d_{w}). The factor $\chi = 1.4414$ is constant for the average cell volume of regular dodecahedral foam, for which the average cell volume ($\bar{V}_{\text{cell}}$) and the edge length (a) are:[S58,S59]

$$\bar{\text{V}}_{\text{cell}} = \frac{1}{4}\left(15 + 7\sqrt{5}\right)a^3 \quad \text{(S58)}$$

$$a = \frac{1}{\sqrt{\frac{5}{2}+\frac{11}{10}\sqrt{5}}}(d_{\text{ins}}) \quad \text{(S59)}$$

In regular dodecahedral foam, each of 12 cell walls is shared by two cells and each of 30 edges is shared by three cells; number density of struts $N_{\text{v,strut}}$ and number density of cell walls $N_{\text{v,wall}}$ can be obtained from:

$$N_{\text{v,wall}} = \frac{12}{2}N_{\text{v,cell}} = 6N_{\text{v,cell}} \quad \text{(S60)}$$

$$N_{\text{v,strut}} = \frac{30}{3}N_{\text{v,cell}} = 10N_{\text{v,cell}} \quad \text{(S61)}$$

S7 Material Properties

To calculate the predicted thermal conductivity and the conductive and radiative contributions of PS and PMMA foams at 300 K and 1 bar, the physical properties of the polymer and air were used in the model. Thermal conductivity of air was taken as 0.026 W m^{-1} K^{-1}, and gaseous refractive index n_g as 1.0, with the extinction coefficient κ_g of 0.[S3,S6] The thermal conductivity of polymer k_s was taken as 0.186 W m^{-1} K^{-1} for PS[S3,S7] and 0.2098 W m^{-1} K^{-1} for PMMA[S61]. The spectral refractive indices $n_{\lambda,s}$ the spectral extinction coefficients $\kappa_{\lambda,s}$, and the spectral dielectric permittivities $\varepsilon_{\lambda,s}$ were adopted from published data measured by FTIR for PS[S62] and PMMA[S63] films.

S8 The Thermal Conductivity of PS and PMMA Foams

The conductive and radiative thermal conductivities of PS and PMMA foams as a function of various cell sizes and void fractions at 300 K are shown in **Figure S3**. Their contributions to the total thermal conductivity are shown in **Figure S4**.

The theoretically predicted values and the measured experimental data for the total thermal conductivity of PS foams[S7,S12,S64–S70] and PMMA foams,[S61,S71–S73] are compared in **Figure S5** and **Figure S6**, respectively.

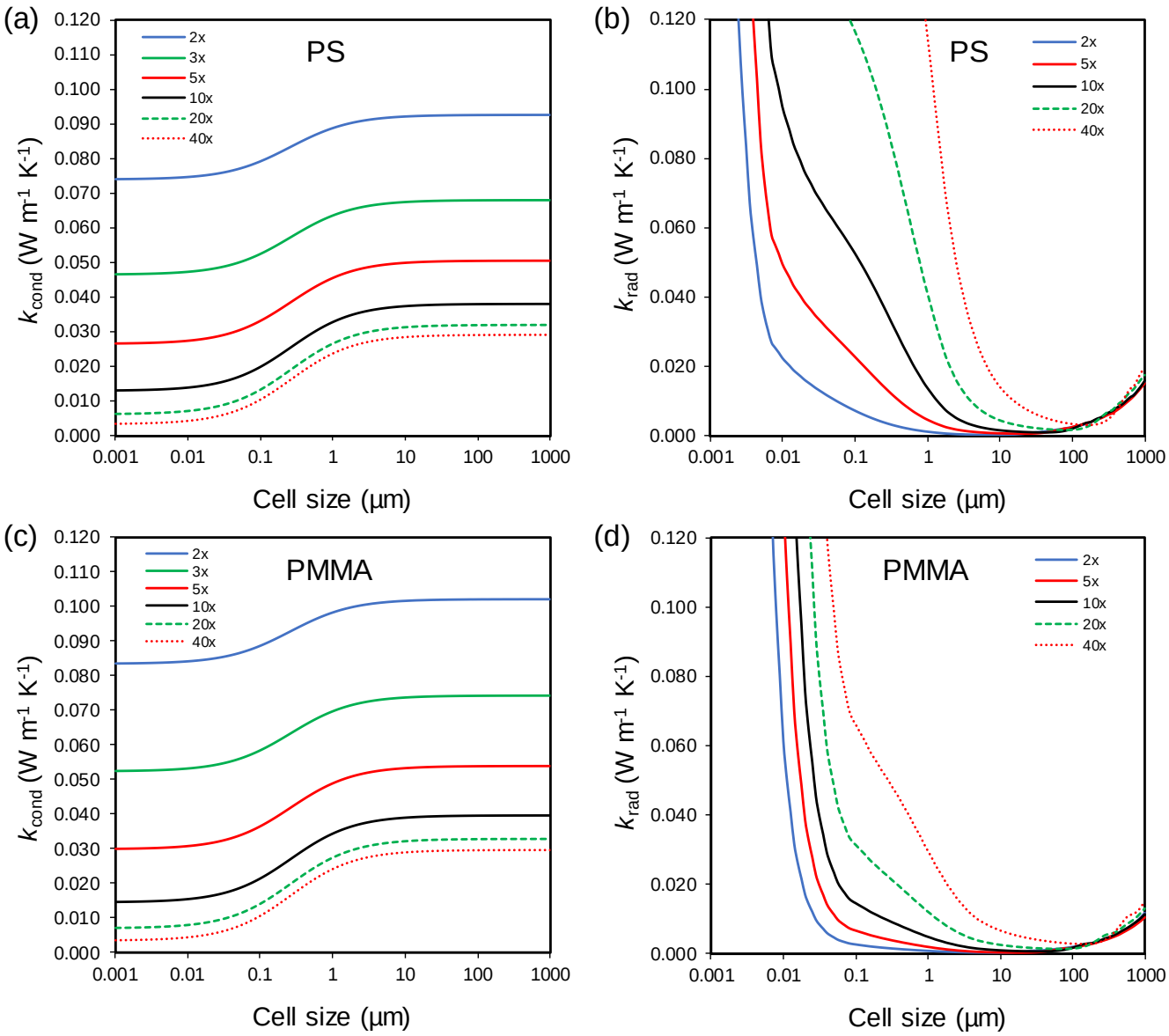

Figure S3. The conductive and radiative thermal conductivities of (a-b) PS and (c-d) PMMA foams as a function of the cell size at various volume expansion ratios.

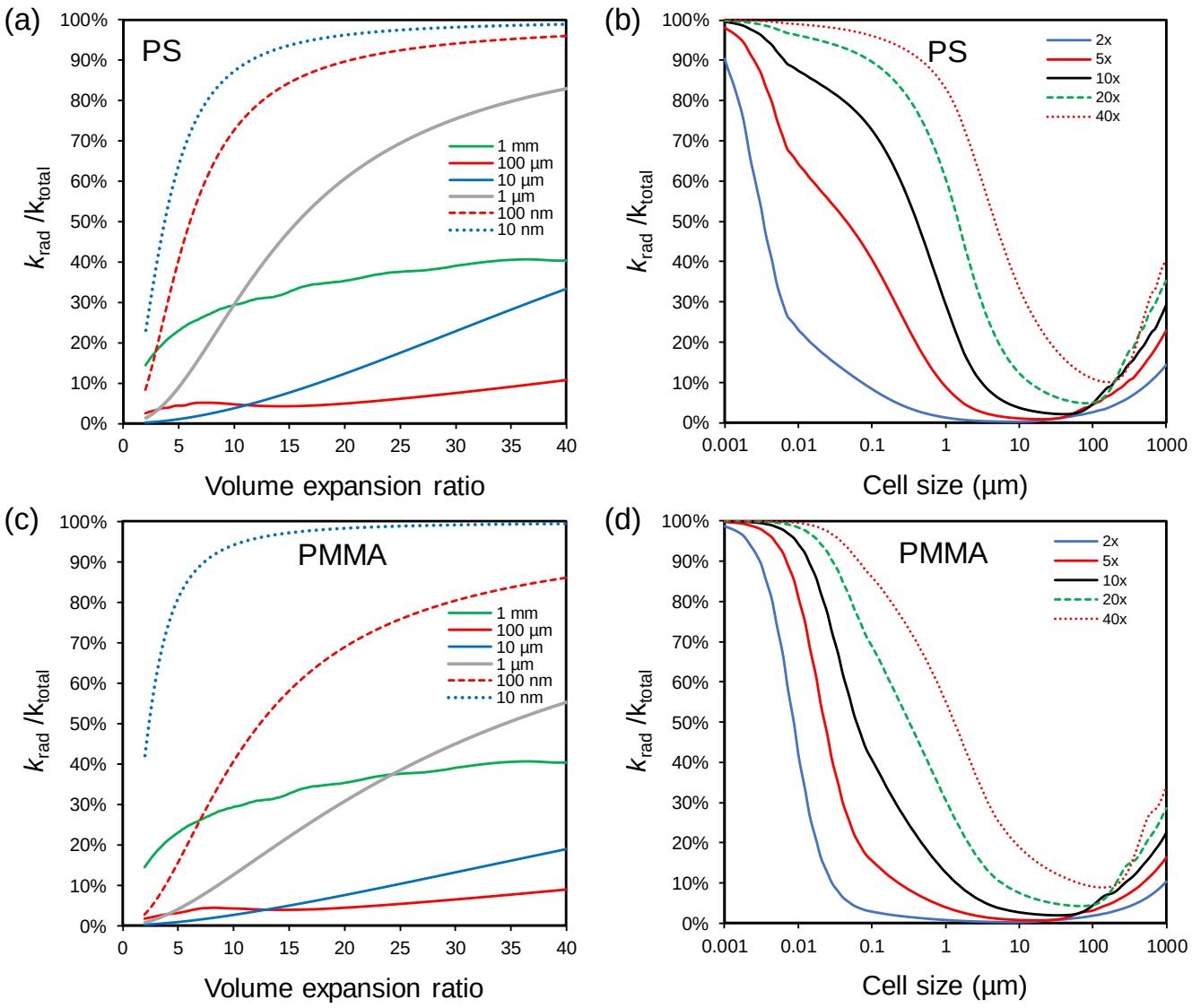

Figure S4. Contributions of radiative heat transfer to the effective thermal conductivity of (a-b) PS and (c-d) PMMA foams at various volume expansion ratios and cell sizes.

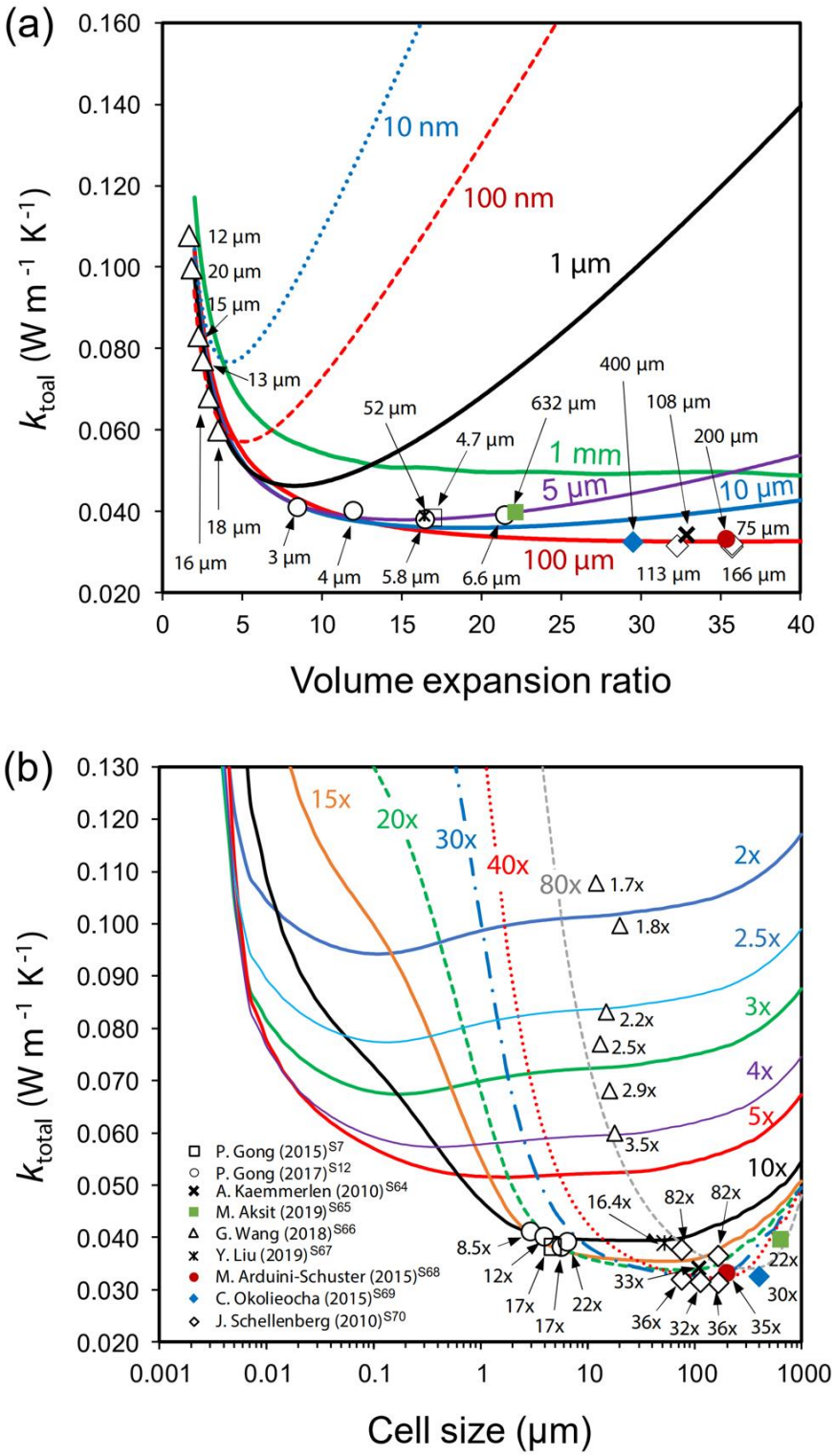

Figure S5. Comparison of the modeling predictions and the experimental data for the total thermal conductivity of PS foams at various expansion ratios and cell sizes.

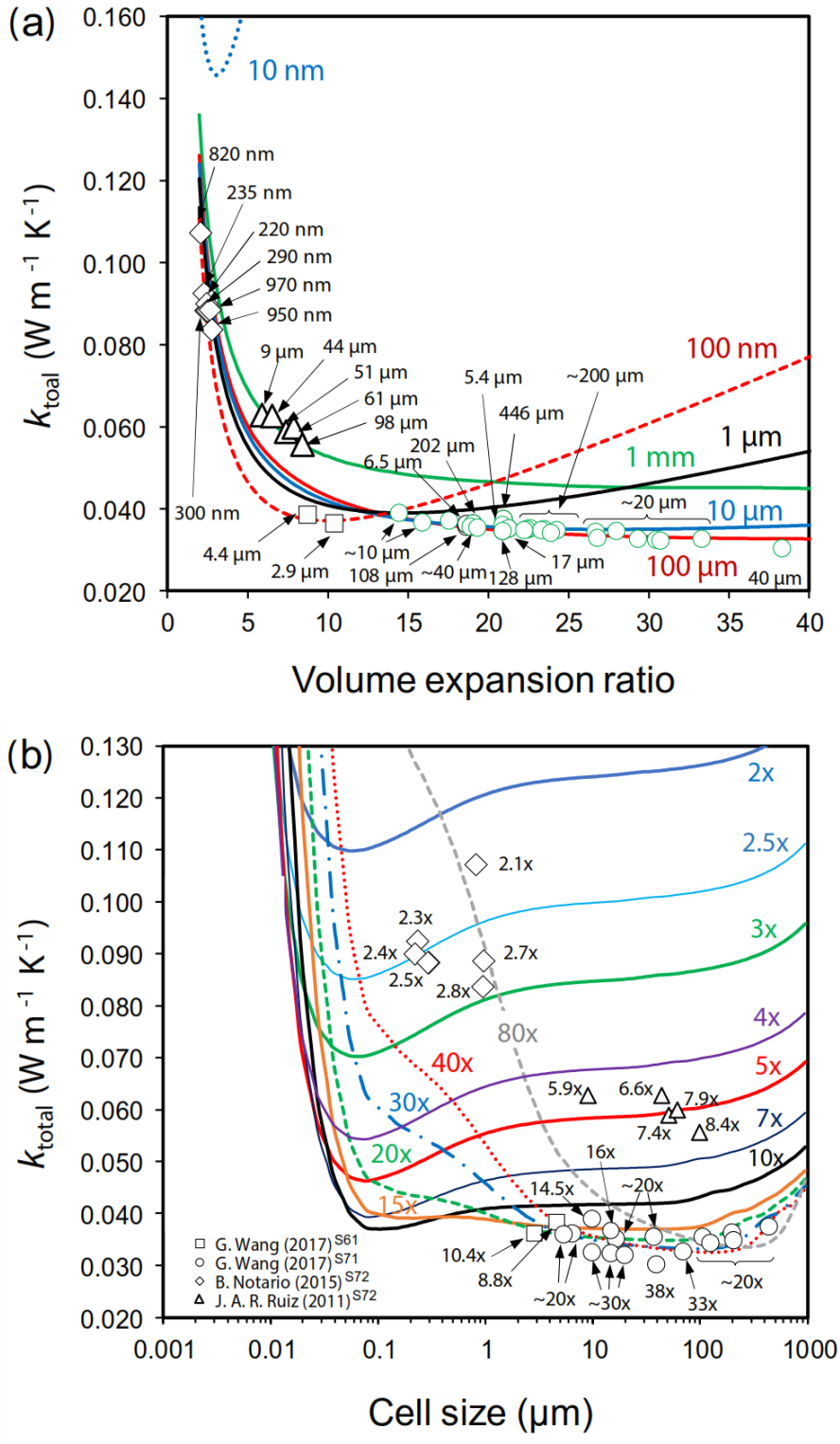

Figure S6. Comparison of the modeling predictions and the experimental data for the total thermal conductivity of PMMA foams at various expansion ratios and cell sizes.

References

S1 A. G. Leach, *J. Phys. Appl. Phys.*, 1993, **26**, 733–739.

S2 H. W. Russell, *J. Am. Ceram. Soc.*, 1935, **18**, 1–5.

S3 G. Wang, C. Wang, J. Zhao, G. Wang, C. B. Park and G. Zhao, *Nanoscale*, 2017, **9**, 5996–6009.

S4 G. N. Dul'nev, *J. Eng. Phys.*, 1965, **9**, 275–279.

S5 M. Knudsen, *Ann. Phys.*, 1911, **339**, 593–656.

S6 Z. M. Zhang, *Nano/microscale heat transfer*, McGraw-Hill, New York, NY, 2007.

S7 P. Gong, P. Buahom, M.-P. Tran, M. Saniei, C. B. Park and P. Pötschke, *Carbon*, 2015, **93**, 819–829.

S8 P. Ferkl, R. Pokorný, M. Bobák and J. Kosek, *Chem. Eng. Sci.*, 2013, **97**, 50–58.

S9 M. Planck, *The theory of heat radiation*, Dover Publications, New York, 1991.

S10 T. H. Boyer, *Am. J. Phys.*, 2018, **86**, 495–509.

S11 J. R. Howell, M. P. Mengüç and R. Siegel, *Thermal radiation heat transfer*, CRC Press, Boca Raton London New York, 6th ed., 2016.

S12 P. Gong., G. Wang, M.-P. Tran, P. Buahom, S. Zhai, G. Li and C. B. Park, *Carbon*, 2017, **120**, 1–10.

S13 G. Mie, *Ann. Phys.*, 1908, **330**, 377–445.

S14 F. Frezza, F. Mangini and N. Tedeschi, *J. Opt. Soc. Am. A*, 2018, **35**, 163.

S15 M. Born and E. Wolf, *Principles of optics: electromagnetic theory of propagation, interference and diffraction of light*, Cambridge University Press, Cambridge; New York, 7th expanded ed., 1999.

S16 R. Siegel, J. R. Howell and M. P. Mengüç, *Thermal radiation heat transfer*, 2016.

S17 J. M. Wallace and P. V. Hobbs, *Atmospheric science: an introductory survey*, Elsevier Academic Press, Amsterdam ; Boston, 2nd ed., 2006.

S18 H. C. van de Hulst, *Light scattering by small particles*, Dover Publications, New York, 1981.

S19 L. R. F.R.S, *Lond. Edinb. Dublin Philos. Mag. J. Sci.*, 1881, **12**, 81–101.

S20 E. Hecht and A. Zając, *Optics*, Addison-Wesley Pub. Co, Reading, Mass, 2nd ed., 1987.

S21 G. Waldman, *Introduction to light: the physics of light, vision, and color*, Dover Publications, Mineola, N.Y, Dover ed., 2002.

S22 A. Borovoi, A. Konoshonkin and N. Kustova, *J. Quant. Spectrosc. Radiat. Transf.*, 2014, **146**, 181–189.

S23 H. Lindqvist, J. Martikainen, J. Räbinä, A. Penttilä and K. Muinonen, *J. Quant. Spectrosc. Radiat. Transf.*, 2018, **217**, 329–337.

S24 L. Bi, P. Yang, G. W. Kattawar, Y. Hu and B. A. Baum, *J. Quant. Spectrosc. Radiat. Transf.*, 2011, **112**, 1492–1508.

S25 A. W. Adey, *Can. J. Phys.*, 1956, **34**, 510–520.

S26 J. R. Wait, *Can. J. Phys.*, 1955, **33**, 189–195.

S27 A. C. Lind and J. M. Greenberg, *J. Appl. Phys.*, 1966, **37**, 3195–3203.

S28 E. W. Montroll and R. W. Hart, *J. Appl. Phys.*, 1951, **22**, 1278–1289.

S29 K. J. Chalut, M. G. Giacomelli and A. Wax, *J. Opt. Soc. Am. A Opt. Image Sci. Vis.*, 2008, **25**, 1866–1874.

S30 J. D. Keener, K. J. Chalut, J. W. Pyhtila and A. Wax, *Opt. Lett.*, 2007, **32**, 1326–1328.

S31 Y. Han, G. Gréhan and G. Gouesbet, *Appl. Opt.*, 2003, **42**, 6621–6629.

S32 P. Chýlek and J. D. Klett, *JOSA A*, 1991, **8**, 1713–1720.

S33 K. A. Shapovalov, *Optics*, 2014, **2**, 32.

S34 J. A. Shaker and D. H. O. Bebbington, in *2017 Progress in Electromagnetics Research Symposium - Fall (PIERS - FALL)*, 2017, pp. 2548–2555.

S35 P. Chýlek and J. D. Klett, *JOSA A*, 1991, **8**, 274–281.

S36 P. Chýlek and G. Videen, *J. Atmospheric Sci.*, 1994, **51**, 175–190.

S37 M. I. Mishchenko, L. D. Travis and A. A. Lacis, *Multiple scattering of light by particles: radiative transfer and coherent backscattering*, Cambridge Univ. Press, Cambridge, 2006.

S38 M. Kerker, in *The Scattering of Light and Other Electromagnetic Radiation*, ed. M. Kerker, Academic Press, 1969, vol. 16, pp. 255–310.

S39 M. F. Modest, in *Radiative Heat Transfer*, Elsevier, 2013, pp. 1–30.

S40 D. D. Baillis, R. Coquard, J. Randrianalisoa, L. A. Dombrovsky and R. Viskanta, *Spec. Top. Rev. Porous Media - Int. J.*, 2013, **4**, 111–136.

S41 A. Kaemmerlen, R. Coquard and D. Baillis, in *International Symposium on Advances in Computational Heat Transfer*, Begellhouse, Marrakesh, Morocco, 2008, pp. 1–14.

S42 E. Placido, M. C. Arduini-Schuster and J. Kuhn, *Infrared Phys. Technol.*, 2005, **46**, 219–231.

S43 A. Cohen and P. Alpert, *Appl. Opt.*, 1980, **19**, 558–560.

S44 S.-C. Lee and G. R. Cunnington, *J. Thermophys. Heat Transf.*, 2000, **14**, 121–136.

S45 A. Cohen, *Opt. Lett.*, 1980, **5**, 150–152.

S46 R. T. Wang and H. C. van de Hulst, *Appl. Opt.*, 1995, **34**, 2811–2821.

S47 G. Kirchhoff, *Ann. Phys. Chem.*, 1860, **185**, 275–301.

S48 G. Kirchhoff, *Lond. Edinb. Dublin Philos. Mag. J. Sci.*, 1860, **20**, 1–21.

S49 P.-M. Robitaille, *Prog. Phys.*, 2009, **4**, 11.

S50 M. Francoeur, M. P. Mengüç and R. Vaillon, *J. Phys. Appl. Phys.*, 2010, **43**, 075501.

S51 M. Francoeur, M. P. Mengüç and R. Vaillon, *Phys. Rev. B*, 2011, **84**, 075436.

S52 S. Basu, *Near-field radiative heat transfer across nanometer vacuum gaps: fundamentals and applications*, William Andrew is an imprint of Elsevier, Cambridge, MA, USA, 2016.

S53 P. J. Mohr, D. B. Newell, B. N. Taylor and E. Tiesinga, *Metrologia*, 2018, **55**, 125–146.

S54 D. B. Newell, F. Cabiati, J. Fischer, K. Fujii, S. G. Karshenboim, H. S. Margolis, E. de Mirandés, P. J. Mohr, F. Nez, K. Pachucki, T. J. Quinn, B. N. Taylor, M. Wang, B. M. Wood and Z. Zhang, *Metrologia*, 2018, **55**, L13–L16.

S55 L. J. Gibson and M. F. Ashby, *Cellular solids structure and properties*, 1997.

S56 M. Antunes, J. I. Velasco, E. Solórzano and M. Á. Rodríguez-Pérez, in *Heat Transfer in Multi-Phase Materials*, eds. A. Öchsner and G. E. Murch, Springer Berlin Heidelberg, Berlin, Heidelberg, 2010, vol. 2, pp. 131–161.

S57 S. Pardo-Alonso, E. Solórzano, L. Brabant, P. Vanderniepen, M. Dierick, L. Van Hoorebeke and M. A. Rodríguez-Pérez, *Eur. Polym. J.*, 2013, **49**, 999–1006.

S58 E. W. Weisstein, *The CRC concise encyclopedia of mathematics*, Chapman & Hall, London, 2011.

S59 H. M. Cundy and A. P. Rollett, *Mathematical models*, Tarquin Publ, St Albans, 3. ed., reprint., 2007.

S60 P. Buahom and S. Areerat, *J. Cell. Plast.*, 2011, **47**, 133–152.

S61 G. Wang, J. Zhao, L. H. Mark, G. Wang, K. Yu, C. Wang, C. B. Park and G. Zhao, *Chem. Eng. J.*, 2017, **325**, 632–646.

S62 J. Liang, M. Tu, G. Cui, W. Liu, Z. Qiao and W. Peng, in *2017 International Conference on Optical Instruments and Technology: IRMMW-THz Technologies and Applications*, eds. L. Dong, X.-C. Zhang, C. Zhang and Z. Huang, SPIE, Beijing, China, 2018, p. 11.

S63 S. Tsuda, S. Yamaguchi, Y. Kanamori and H. Yugami, *Opt. Express*, 2018, **26**, 6899.

S64 A. Kaemmerlen, C. Vo, F. Asllanaj, G. Jeandel and D. Baillis, *J. Quant. Spectrosc. Radiat. Transf.*, 2010, **111**, 865–877.

S65 M. Aksit, C. Zhao, B. Klose, K. Kreger, H.-W. Schmidt and V. Altstädt, *Polymers*, 2019, **11**, 268.

S66 G. Wang, G. Zhao, G. Dong, L. Song and C. B. Park, *J. Mater. Chem. C*, 2018, **6**, 12294–12305.

S67 Y. Liu, L. Jian, T. Xiao, R. Liu, S. Yi, S. Zhang, L. Wang, R. Wang and Y. Min, *Polymers*, 2019, **11**, 985.

S68 M. Arduini-Schuster, J. Manara and C. Vo, *Int. J. Therm. Sci.*, 2015, **98**, 156–164.

S69 C. Okolieocha, T. Köppl, S. Kerling, F. J. Tölle, A. Fathi, R. Mülhaupt and V. Altstädt, *J. Cell. Plast.*, 2015, **51**, 413–426.

S70 J. Schellenberg and M. Wallis, *J. Cell. Plast.*, 2010, **46**, 209–222.

S71 G. Wang, J. Zhao, G. Wang, L. H. Mark, C. B. Park and G. Zhao, *Eur. Polym. J.*, 2017, **95**, 382–393.

S72 B. Notario, J. Pinto, E. Solorzano, J. A. de Saja, M. Dumon and M. A. Rodríguez-Pérez, *Polymer*, 2015, **56**, 57–67.

S73 J. A. Reglero Ruiz, C. Saiz-Arroyo, M. Dumon, M. A. Rodríguez-Perez and L. Gonzalez, *Polym. Int.*, 2011, **60**, 146–152.